Experimental optical imaging during pancreatic cancer interventions

Manen, L. van

Chapter 11

Detection of cutaneous oxygen saturation using a novel snapshot hyperspectral camera: a feasibility study

L. van Manen, W.A.J. Birkhoff, J. Eggermont, R.J. Hoveling, P. Nicklin, J. Burggraaf, R. Wilson, J.S.D. Mieog, D.J. Robinson, A.L. Vahrmeijer, M.S. Bradbury, J.Dijkstra

Quantitative Imaging in Medicine and Surgery. 2021 Sep;11(9):3966-3977.

Abstract

Background

Tissue necrosis, a consequence of inadequate tissue oxygenation, is a common post-operative complication. As current surgical assessments are often limited to visual and tactile feedback, additional techniques that can aid in the interrogation of tissue viability are needed to improve patient outcomes. In this bi-institutional pilot study, the performance of a novel snapshot hyperspectral imaging camera to detect superficial cutaneous oxygen saturation (StO_2) was evaluated.

Methods

Healthy human volunteers were recruited at two participating centers. Cutaneous StO_2 of the forearm was determined by a snapshot hyperspectral camera on two separate study days during occlusion-reperfusion of the brachial artery and after induction of local vasodilation. To calculate the blood StO_2 at each pixel in the multispectral image, spectra were selected, and fitting was performed over wavelengths ranging from 470 to 950 nm.

Results

Quantitative detection of physiological changes in cutaneous StO_2 levels was feasible in all sixteen volunteers. A significant ($P<0.001$) decrease in cutaneous StO_2 levels from 78.3% (SD:15.3) at baseline to 60.6% (SD:19.8) at the end of occlusion phase was observed, although StO_2 levels returned to baseline after five minutes. Mean cutaneous StO_2 values were similar in the same subjects on separate study days (Pearson R^2: 0.92 and 0.77, respectively) at both centers. Local vasodilation did not yield significant changes in cutaneous StO_2 values.

Conclusions

This pilot study demonstrated the feasibility of a snapshot hyperspectral camera for detecting quantitative physiological changes in cutaneous StO_2 in normal human volunteers, and serves as a precursor for further validation in perioperative studies.

Introduction

The restoration of normal tissue function and wound healing following surgery is critically dependent on tissue oxygen saturation (StO_2) and perfusion, among other factors. Tissue ischemia and soft tissue necrosis, caused by inadequate tissue oxygenation, commonly occurs in patients with (micro)vascular diseases requiring surgical interventions. However, in the post-operative period, wound complications can arise, such as tissue necrosis that necessitates a second surgical procedure. Traditionally, surgeons use tactile and visual feedback, sometimes in combination with handheld Doppler ultrasound, for intraoperatively evaluating tissue perfusion. Nevertheless, healing complications can occur, for instance, in up to 8 and 15% of patients undergoing breast reconstructive surgery or surgical amputations (i.e., below-the-knee), respectively.[1,2] Therefore, additional techniques that can reliably monitor perfusion and oxygenation status in post-operative settings and accurately predict and stratify patients at-risk for delayed surgical wound healing are essential for timely surgical management and for improved quality of life.

Although, transcutaneous oxygen saturation mapping ($TcPO_2$) and optical coherence tomography (OCT) are techniques that could be used for StO_2 monitoring, only $TcPO_2$ is currently used as a standard of care procedure. Both techniques can measure StO_2 levels *in vivo* by detecting optical absorption coefficient differences between oxygenated and deoxygenated haemoglobin.[1,3] However, these techniques have a limited field of view and require contact with the tissue for accurate assessments. Therefore, handheld cameras with a larger field of view, but not requiring direct skin contact, may serve as a practical alternative, in addition to being readily implemented in the perioperative setting.

One emerging technique is hyperspectral imaging, which has been used for biomedical applications, including the assessment of tumour margins and detection of tissue StO_2 in pathologic conditions.[4-6] This device detects the skin diffuse reflectance spectrum of light reflected from tissues after it has been scattered and absorbed by tissue chromophores, such as haemoglobin, fat, or water illuminated with a full spectrum light source.[4] Current available camera systems are mostly push-broom or band sequential scanners, which are limited by the long acquisition times needed to sequentially acquire spectral wavelength bands, precluding real-time imaging evaluations. Therefore, snapshot hyperspectral cameras have recently evolved to address this drawback. The first *in vivo* application of such a snapshot hyperspectral camera system was demonstrated by Gao et al. for the detection of retinal StO_2 levels.[7,8]

We have developed a novel snapshot hyperspectral imaging camera with a large field of view as a prototype system for non-invasively interrogating superficial anatomic structures and for monitoring changes in microvascular perfusion and oxygenation. This feasibility study herein aims to explore the novel capabilities of this hyperspectral snapshot camera system for detecting quantitative physiological changes in cutaneous StO_2 in healthy human volunteers under ambient light conditions, and without the need for direct skin contact.

Material and Methods

Study design

This study was an open observational multicenter feasibility study at the Leiden University Medical Center (LUMC), The Netherlands, and Memorial Sloan Kettering Cancer Center (MSKCC), USA. Healthy human volunteers, equally divided between these Centers, were recruited for participation in this study. Informed consent was obtained from all patients. All patients had a normal Body Mass Index (between 18.5 and 29,9 kg/m2)[9], were not taking medications, and had no past medical history. The study exclusion criteria were hypertension, regular tobacco use, and any confirmed allergies to medications. Furthermore, alcohol and caffeine consumption were prohibited within 12 hours of initiating each imaging session.[10,11] Approval for conducting the clinical trial was obtained at both Centers from their Institutional Review/Regulatory Boards. This trial was registered at the Dutch Trial Register (NL6381).

Study population

Sixteen human volunteers, equally divided between trial sites, were included in this feasibility study. Subject demographics are provided in Table 1. Age, vital signs (basal blood pressure, heart rate), and the BMI, were in the range of those measured in normal healthy adults, and were similar in both patient cohorts. Skin temperatures between cohorts showed statistically significant differences (32.2 [1.1] versus 36.0 [0.5] °C; $P<0.001$). Skin types, assessed according to the Flitzpatrick scale, were similar between the two groups ($P=0.637$).

Hyperspectral imaging system

A snapshot hyperspectral camera system (Hyperea, Quest Medical Imaging B.V., Middenmeer, The Netherlands), which acquires 41 spectral bands across the visual (VIS) and near-infrared (NIR) spectrum, ranging between 470 and 950 nm, was used for image acquisition.[12] The camera system consists of three sensors (RGB, VIS and NIR), which are combined to facilitate simultaneous colour and spectral imaging. The effective sensor resolution is 2048 x 1080 pixels. The spectral bands are acquired using two mosaic sensors, one (4x4 filter pattern) having a spectral range of 470 - 630 nm, and one sensor (5x5 filter pattern) having a spectral range of 600 – 950 nm (Figure 1). This hyperspectral camera system is based on a tiled-filter approach where pixels are individually filtered with narrow Fabry-Pérot bandpass filters (bandwidth ≈ 12 nm each). The camera sensors are pixel aligned on the prism, with a maximum deviation of 1/3 pixel. In this study a camera lens of 35 mm with an aperture size of f/2.8 was used. The camera allows real-time imaging at video frame rates (max. frame rate: 16 frames per second) without the need to scan in either the x- or y- direction. The camera lens was 35 mm. The field of view of the camera is 5 by 10 cm using a 40 cm working distance, which makes this system suitable for clinical use. A signal to noise ratio of maximum 14 could be achieved. The hyperspectral imaging set-up used for this study has four 50 Watt halogen light sources (Philips Lighting B.V., Eindhoven, The Netherlands), which were mounted on the top of a black box, for optimal control of the lighting conditions (Figure 1).

Laser speckle contrast imager

For superficial skin perfusion analysis, a Laser Speckle Contrast Imager (LSCI) (PSI; Perimed, Järfälla, Sweden) was used at one participating center (LUMC). This non-invasive technique is capable of detecting the subcutaneous movement of light-scattering particles.[13,14] The measurement depth of the LSCI device is approximately 0.5 mm. The system uses a divergent laser beam with a

wavelength of 785 nm. Measurements were performed on an area of 3x3 cm, with a frequency of 22 images per second (averaged for capsaicin snapshots). Point density was normal (resolution 0.45 mm). The LSCI data obtained were analysed using PIMsoft software (Perimed, Järfälla, Sweden).

Imaging procedure

To assess the imaging characteristics of the hyperspectral camera, its output was compared with contact measurements obtained using a fiber optic probe and multi-diameter reflectance spectroscopy.[15,16] During each measurement, the reflectance spectra are collected at effective diameters of 200, 600, and 1000 µm; StO_2, and blood volume fraction, was determined using the largest effective single fiber diameter with an interrogation depth of approximately 500 µm.[17] The pathlength of light in the interrogated volume for the point spectroscopy is fixed by the fiber (equal to approximately ½ the fiber diameter). For hyperspectral imaging, the illumination spot size is similar to that of the spectroscopy measurements but longer pathlength light from other points elsewhere are present in the illuminated field of the snapshot camera. Occlusion-reperfusion experiments were performed to characterize tissue optical properties. In each human volunteer, baseline skin StO_2 measurements were made of the right forearm over a two-minute interval. After acquiring these measurements, StO_2 of the right forearm was monitored for five minutes following occlusion of the right brachial artery; this procedure was repeated during the subsequent reperfusion period. In total, the arms of the included subjects did stay for 12 minutes in front of the camera and lamps during the occlusion-reperfusion experiments. Both snapshot images and spectroscopy measurements were taken every 30 seconds, except for the first minute after reperfusion, during which phase images and measurements were taken every second.

To validate this technique, human volunteers were recruited to undergo occlusion-reperfusion at two separate times, separated by more than three days. The patients' vital signs were obtained, namely their blood pressure, heart rate, basal finger oxygenation, and skin temperature, at the start of the measurements. Occlusion-reperfusion experiments were performed, as described above. Hereafter, capsaicin cream, a vasodilator, was applied on the right forearm. It works by activating the vanilloid type-1 receptor that, in turn, results in cutaneous vasodilation.[18] Capsaicin was administered on the same arm over an area of 3 by 3 cm, with an average distance of 5 cm under the radiocarpal joint, after the occlusion-reperfusion measurement. However, this was done only after the subject had rested for approximately 15 minutes, thereby restoring normal cutaneous blood flow. Subsequently, and before the capsaicin challenge, surgical tape was placed about the region of interest (ROI) to prevent spillage of capsaicin beyond the region of application. Thirty minutes after application of the crème, it was removed from the skin, and a superficial skin StO_2 measurement was acquired over a 30-minute time interval, with snapshots taken every 5 minutes. Results were compared with those of control regions located on the same forearm. In the LUMC cohort, blood flow was imaged simultaneously using LSCI.

Data processing

Due to the configuration of the 4x4 and 5x5 mosaic in the sensors and the different offsets that are applied for the placement of this mosaic pattern on the sensor pixels, specific demosaicing of the sensor information into the different spectral datacube components was required. By comparing the differences between the different planes in the spectral datacube, the alignment, cropping and scaling of the sensor data could be optimized. Based on the filter characteristics of both the sensors and the filters in the

camera system, a camera-specific correction matrix could be generated for the correction of the spectral artifacts that occur due to the configuration of the filters on the sensor pixels and the nature of the interference filters, e.g. crosstalk and higher-order transmission. The correction matrix for the spectral data was validated with reference spectra (Figure 1). Next, acquired images were normalized using white and dark reference images, as previously described by Lu et al.[4] Furthermore, a correction for the second-order light effect due to light diffraction [19], provided by the manufacturer, was performed after the normalization of images. Lastly, in order to calculate the blood StO_2 at each pixel in the hyperspectral images, all spectral bands (N=41) were selected in the full range of 470 - 950 nm to enable fitting using a method described previously, although implemented for hyperspectral imaging. [17,20,21] Reflectance spectra were analyzed using an analytical model to describe the wavelength-dependent optical properties to extract physiological and morphological information from the sampled tissue as previously described.[17] In short, attenuation due to absorption within the tissue is modeled using a modified Beer–Lambert law and is a function of both the tissue absorption coefficient (μ_a) and the single fiber photon path length. The reflectance amplitude, as well as the single fiber photon path length, depend on the scattering properties of the tissue, with a dependence on the reduced scattering coefficient (μ'_s) and on the angular distribution of scattering (phase function). Our initial model assumed that absorption was attributable to oxygenated and deoxygenated hemoglobin confined within the local microvasculature. A Levenberg–Marquardt algorithm was used to estimate the parameter values for the microvascular hemoglobin StO_2, the blood volume fraction and average blood vessel diameter by minimizing the chi-squared metric between measured reflectance data and model predictions.[17] Confidence intervals on parameter estimates were calculated from the square root of the diagonal of the covariance matrix.[9] Parameter values were averaged over repeated measurements, weighted by the confidence interval of individual spectral fits, and reported with the associated weighted standard deviation.

This fitting method assumed that blood is the dominant absorber in the field-of view, and that each wavelength travels an equal pathlength in the tissue with scattering losses approximately equal across the wavelength range of interest. The wavelength dependence of the penetration depth is not a confounding factor for the spectroscopy measurements because the fiber (probe) determines the penetration depth and is approximately equal over the wavelength range measured. This is not the case for the hyperspectral camera where longer wavelength photons also contribute to the acquired signal. We determined the effective light collection area of the camera system to be approximately 320 by 320 microns per pixel. StO_2 fitting was performed using software developed in-house, written in C++ programming language. It has been shown that the recovery of blood StO_2 in patients with skin types 1-3 is not affected by skin type.[15] Hyperspectral data were not corrected for skin type. Saturation maps were converted to color-based maps for improved interpretation (blue: low StO_2; red: high StO_2). The fitted StO_2 was not allowed to be greater than 100%, nor lower than 0%, for both spectroscopy and the hyperspectral camera system. The StO_2 maps were imported into MeVisLab (MeVis Medical Solutions AG, Bremen, Germany), and skin StO_2 subsequently calculated based on selecting corresponding ROI, which were located on a planar surface of the forearm and marked with a dermatological marker at the beginning of each measurement procedure. For all analyses, the marked area on the volar side of the forearm was chosen as the ROI. Care was taken during the repeated measurements to choose an ROI as close as possible to

the previous used ROI, using the LSCI and hyperspectral images as reference. In the analysis software, the ROI was manually selected using the dermatological markers as reference point.

Statistical analysis

Continuous variables were presented as mean values + standard deviations ([SD]) in normal distributed data or as median values (interquartile range [IQR]) in non-normal distributed data, respectively. The Mann-Whitney U-test, independent t-test, paired t-test and ANOVA test were used for comparison of continuous variables. For categorical variables, a Chi-Squared test was used to compare groups. Correlations were calculated by using the mean correlation coefficient (Pearson R^2). Correlation coefficients were interpreted according to Schober et al.[22] A P-value below 0.05 (two-sided) was considered statistically significant. SPSS Statistics for Windows, version 23.0 (IBM Corp., Armonk, N.Y., USA) was used for the statistical analysis. Graphs were created using Graphpad 8.0 (GraphPad Software, Inc., San Diego, CA).

Results

Spectral fitting

Figure 2 shows the variation in the percentage (%) of StO_2 measured using single fiber reflectance and hyperspectral imaging. The baseline StO_2 measured before occlusion using the fiber optic reflectance technique is significantly lower than that using hyperspectral imaging, but is consistent with previous measurements in the skin of the inner forearm.[15] During occlusion, the skin blood volume fraction is reduced (data not shown); consequently, there are large confidence intervals on these data points. Upon reperfusion, blood volume increases and subsequently returns to near baseline levels; in this regime, no significant differences in StO_2 levels were found using these measurement techniques. However, it is important to note that there are substantial uncertainties in both measurements of StO_2 due to the relatively low blood volume in the interrogated region, as we have described previously.[9]

Occlusion-reperfusion experiments

Measurement of StO_2 levels using a linear fitting algorithm was feasible in all volunteers during all phases of occlusion and reperfusion. General analysis showed a statistically significant ($P<0.001$) decrease in cutaneous StO_2 levels from 78.3% (SD: 15.3) at baseline to 60.6% (SD: 19.8) at the end of occlusion phase (Figure 3). Subgroup analysis showed that baseline StO_2 differed significantly between the subjects recruited at LUMC and MSKCC (mean StO_2: 69.9 versus 86.6 %, $P<0.001$), with a decrease in StO_2 of 20.3 and 14.3 %, respectively. Overall StO_2 levels returned to baseline at the end of the reperfusion phase, which was after 12 minutes (mean StO_2: 70.4 versus 85.1 %, for the two cohorts respectively). An additional perfusion analysis was performed in the LUMC cohort using LSCI and showed a strong correlation (Pearson R^2: 0.86) of blood flow with StO_2 levels during occlusion-reperfusion phases (Figure 4).

Moreover, StO_2 correlations between the two measurement days were analysed, resulting in an overall Pearson R^2 of 0.85, although a higher correlation was observed in the LUMC cohort (Pearson R^2: 0.92)

compared to the MSKCC cohort (Pearson R^2: 0.77). Individual analyses of all patients showed an excellent correlation in 13 (81%), a strong correlation in 2 (13%) and a fair correlation in 1 (6%) subject.

Effect of local vasodilatation

After application of capsaicin cream, statistically significant increases in blood flow due to vasodilatation (P<0.001) were measured (with LSCI) within the most superficial layers of the skin; blood flow increased from 76.7 (SD:11.1) to 146.9 (SD: 38.4) arbitrary units (AU). However, cutaneous StO_2 did not change significantly (P=0.927) after application of capsaicin in the most superficial layers (Figure 5). Nevertheless, mean StO_2 levels in the MSKCC cohort were significantly (P<0.001) higher compared to the LUMC cohort.

Discussion

In this multicenter study, we explored the feasibility of a novel snapshot hyperspectral camera system for non-invasive detection of superficial cutaneous StO_2 under different physiological conditions in normal, healthy human volunteers. Strong correlations were found between the StO_2 measurements acquired during occlusion-reperfusion experiments. Furthermore, local vasodilation did result in an increased cutaneous vascular flux, but not in a significantly higher tissue StO_2 level in the most superficial layers of the skin.

In general, non-invasive imaging using endogenous contrast for the detection and monitoring of cutaneous StO_2 levels is advantageous, and may offer distinct benefits over methods requiring injection of exogenous contrast agents for specific indications. In the perioperative setting, there is a general lack of real-time non-invasive imaging tools for reliably monitoring alterations in perfusion and oxygenation status. In the future, such tools could potentially improve patient care outcomes by their ability to detect decreased StO_2 about surgical margins, wound sites, and sites of graft placement, for instance, in addition to guiding clinical management. Moreover, direct skin contact is not needed for such measurements. To our knowledge, this is the first study implementing an existing and validated algorithm for quantitatively analysing cutaneous StO_2 by utilizing a snapshot hyperspectral camera system in human subjects. Recently, more systems have been introduced into the clinic for StO_2 monitoring of the bowel, skin and cerebral cortex.[23-27] Current available hyperspectral camera systems have longer acquisition times than those used by this snapshot hyperspectral camera system, precluding the types of evaluations performed herein. Moreover, other camera systems lack the ability to quantitatively monitor changes in tissue StO_2 by using relative oxyhemoglobin or deoxyhemoglobin measurements as surrogate markers for tissue StO_2. Our data supports the hypothesis that quantitative cutaneous StO_2 imaging is feasible and reproducible with good correlations in human volunteers. This is also underlined by the fact that the performance of this system was independently evaluated at two different centers.

However, a few limitations are noteworthy. First, as the study recruited a relatively small number of normal, healthy human volunteers, the results may not be representative of larger patient populations, who may exhibit a variety of baseline characteristics. Second, the hyperspectral camera system has 41 wavelength bands divided over two mosaic sensors, which implies a lower spatial resolution (i.e., either

2 or 2.5 times) that of the original resolution, noted earlier, although this was found not to be a limiting factor in the current study. Furthermore, we decided to use contact point optical spectroscopy as a reference for comparing the StO_2 of the most superficial layers of tissue. Based on these comparisons, a fitting algorithm was proposed, in order to quantify StO_2, which has been validated in other clinical studies.[21] Nevertheless, we acknowledge that other reference hyperspectral imaging devices suitable for StO_2 detection could have also been used to supplement the perfusion data obtained by LSCI, which was unfortunately only performed one center. Moreover, a general drawback of hyperspectral imaging is that penetration depths of only several hundred micrometres to a maximum of multiple millimetres can be interrogated, which are wavelength-dependent, limiting the applicability of this optical tool to assessments of the most superficial layers of the target tissue of interest (up to the dermis at the red end of the spectrum).[28] Nevertheless, compared to contact point spectroscopy, it seems that the sampling depth is greater for the hyperspectral camera, resulting in higher StO_2 values (Figure 2). The simple linear model of light transport in tissue we have used in the present study is based on assumptions that the scattering remains constant, and that the pathlength travelled is equal for all photons over the wavelength range of interest. The reduced scattering coefficient is known to vary across the visible spectrum. This means that the calculated absorbance of the tissue may be overestimated at the red end of the spectrum. Furthermore, the algorithm did not account for the effect of melanin, as it is very difficult to separate the influence of scattering and the absorption due to melanin without measuring in the blue-green portion of the visible spectrum. Finally, alterations in penetration depth and sampling volume may occur during occlusion, given that the distribution of absorbers changes. While these changes were not accounted for in our analysis, it was felt that the scattering properties of tissues in the forearm would not be significantly affected by occlusion remote from that site.

A high inter-patient variability in cutaneous StO_2 values was observed in this study, both within and across patient cohorts, however the differences in StO_2 values were not significant between the two measurement days in both cohorts, which was also demonstrated by a Pearson R^2 value of 0.85. Controversial data has been published for baseline cutaneous StO_2 values in the range of 50-96%, depending on the camera system used and region of interest in which the measurement was taken.[27,29-32] One explanation for the differences in StO_2 within cohorts may be attributed to gender differences. For example, in the LUMC cohort, females tended to have a higher baseline StO_2 or more subcutaneous fat. It has been demonstrated that fatty tissues are relatively poorly oxygenated, although the BMI included for all volunteers was within the normal range.[9,33] A high inter-patient variability may also be attributed to known wavelength-dependent and depth-dependent variations in cutaneous StO_2 values, that is, superficial skin layers exhibit lower StO_2 values than those found for the well-perfused deeper tissue layers. Another possible explanation is that skin temperature might have led to differences in cutaneous StO_2 between the two cohorts, as this parameter was significantly different at baseline. The large differences in baseline StO_2 between both cohorts could probably be explained by the room temperature, which was significantly higher at MSKCC, leading to increased vasodilatation with subsequent higher StO_2 levels, as previously demonstrated.[31] Moreover, the skin temperature could have been affected by the heat of the light sources, although StO_2 levels in both groups were similar at the beginning and at the end of the measurement period. Interestingly, capsaicin interventions did not result in significantly higher StO_2 levels for either patient cohort. Through activation of the TLPRV1 receptor, capsaicin is known to cause an increased neurogenic vasodilation (amongst other

responses, such as flare, pain, heat, and cutaneous hypersensitivity). This challenge showed that a flare and increased vasodilation did not significantly influence StO_2 measurements, which might be explained by the fact that healthy volunteers are already well oxygenated under normal circumstances and consequently the effect of local vasodilation is minimal. Nevertheless, there is still a trend towards higher saturation levels after application of capsaicin, however due to the expected limited effect on the StO_2 and the small sample size of our study, the detected StO_2 values are not changed significantly.

Besides hyperspectral imaging, other non-invasive techniques for StO_2 mapping, such as optical coherence tomography (near-infrared) spectroscopy, or photoacoustic imaging can be used, although these techniques have significant shortcomings, including the offering of only a limited field of view and/or an inability to acquire imaging data, respectively.[3,34] Recently, another imaging technique termed Single Snapshot of Optical Properties (SSOP), which is based on the Spatial Frequency Domain Imaging (SFDI) principle, allows real-time quantitative imaging of tissue oxygenation.[35,36]

Future work will focus on developing a more user-friendly system and evaluating other sources for better controlled light conditions. Furthermore, data analysis steps and software will be improved to enable real-time intraoperative StO_2 mapping, as current frame rate settings are only about 16 frames per second. Additional refinements, such as mounting the camera head, including light sources, on a stable arm, are needed to efficiently translate and implement such a prototype system into a variety of clinical settings. Importantly, StO_2 measurements are expected to be similar for both elderly adults and younger individuals.[21] In this proof-of-concept study, we focused on the assessment of cutaneous oxygenation status. For intraoperative applications, however, additional technical issues that may limit accuracy e.g., variations in skin thickness, would need to be addressed. In the present work, we attempted to minimize such contributions by imaging the inner aspect of the arm. Different applications and clinical conditions may necessitate specific mechanical solutions to be advanced, which will need to be evaluated and tested. These additional capabilities, however, would also enable high-resolution, full-field StO_2 imaging to be combined, in the same setting, with other real-time imaging strategies, such as fluorescence imaging that utilizes near-infrared wavelengths for the visualisation of multiple fluorophores. Such a hybrid system could also potentially allow for the simultaneous assessment of tissue StO_2 and perfusion. As this camera system has only been evaluated in healthy volunteers, it will be necessary to validate its clinical utility in a more heterogenous patient population. Future implementation will therefore focus on assessing feasibility under clinical circumstances such as patients with vascular conditions arising from, for example, diabetes mellitus, or during reconstructive surgical procedures.

Conclusions

In conclusion, this early-stage multicenter clinical trial demonstrated the feasibility of utilizing a novel snapshot hyperspectral camera system for the detection of cutaneous StO_2 in normal, healthy human volunteers. These findings are being used to inform next-stage camera system developments for monitoring oxygenation status in both non-surgical oncologic and peri-operative settings. In these settings, patients with vascular disease might potentially be risk-stratified for improving clinical decision-making and outcomes.

Table 1. Demographics of study population and overall results of cutaneous oxygen saturation measurements.

	LUMC cohort (N=8)	MSKCC validation cohort (N=8)	*P*- value
Sex, male (%)	4 (50)	2 (25)	0.302
Age (year), median (IQR)	23.5 (22.3-24.0)	23.5 (21.3-38.0)	0.798
BMI (kg/m^2), mean (SD)	24.6 (2.7)	23.3 (2.4)	0.348
Blood pressure, mean (SD)			
Systolic	120 (6.1)	119 (9.9)	0.834
Diastolic	77 (7.7)	73 (5.3)	0.309
Skin temperature (°C), mean (SD)	32.3 (1.1)	36.0 (0.5)	<0.001
Heart rate (BPM), mean (SD)	77 (16.5)	81 (11.8)	0.497
Skin type flitzpatrick (n, %)			
I	3 (37.5)	2 (25.0)	0.637
II	3 (37.5)	5 (62.5)	
III	1 (12.5)	1 (12.5)	
IV	1 (12.5)	-	
V	-	-	
VI	-	-	
Cutaneous StO_2, mean (SD)			
Basal phase	69.9 (15.3)	86.6 (10.0)	<0.001
Max. Occlusion	49.6 (16.5)	72.3 (15.9)	
Reperfusion	70.4 (16.4)	85.5 (9.9)	

Abbreviations: IQR: interquartile range; SD: standard deviation; BMI: body mass index; BPM: beats per minute; StO_2: oxygen saturation.

Figure 1. Overview of the hyperspectral snapshot camera system and its specifications. Images of the forearm of human volunteers were acquired by the hyperspectral snapshot camera, which was mounted in a black box containing four halogen light (broad band illumination) spots on top of each corner (A). The spectral response covers the wavelength range of 470-630 nm for the VIS sensor and 600-950 nm for the NIR sensor (B). The experimental prototype of the camera consists of three camera sensors (RGB-VIS-NIR) which are pixel aligned on the prism [37,38] and a 35 mm lens with a f/2.8 aperture (C). The camera is based on a tiled filter approach where pixels are individually filtered with narrow Fabry-Pérot bandpass filters (bandwidth ≈ 12 nm each). Each image acquisition leads to a hypercube with a spatial resolution of 2048 x 1080 pixels and 41 spectral bands after processing (D).

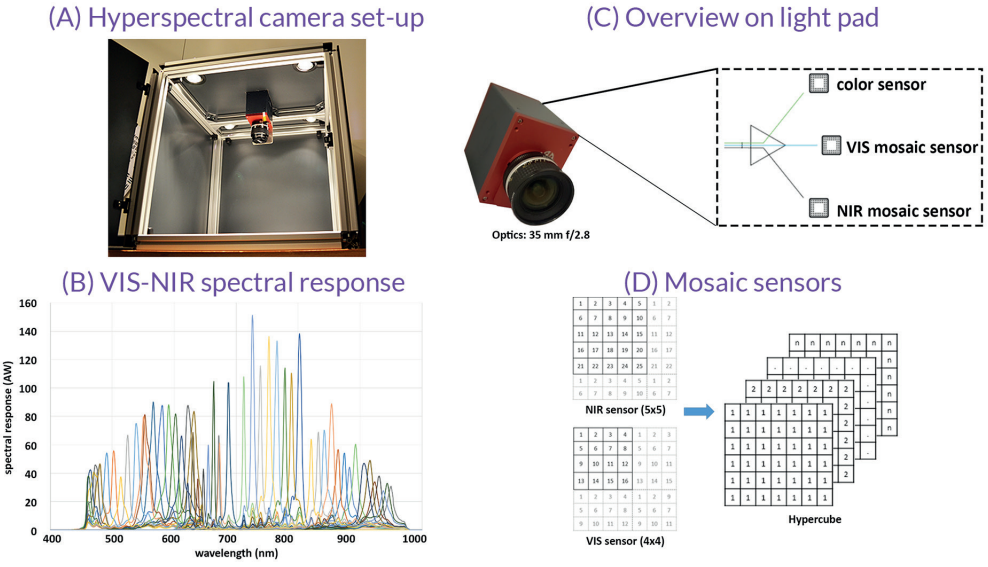

Figure 2. Comparison of single fiber reflectance spectroscopy with hyperspectral imaging for blood oxygen saturation (StO_2) detection. It shows the variation in the percentage (%) of StO_2 measured using single fiber reflectance and hyperspectral imaging. The baseline StO_2 measured before occlusion using the fiber optic reflectance technique is significantly lower than that using hyperspectral imaging. During occlusion, the skin blood volume fraction is reduced. Upon reperfusion, blood volume increases and subsequently returns to near baseline levels. It is important to note that there are substantial uncertainties in both measurements of StO_2 due to the relatively low blood volume in the interrogated region. *Abbreviation: StO_2: oxygen saturation.*

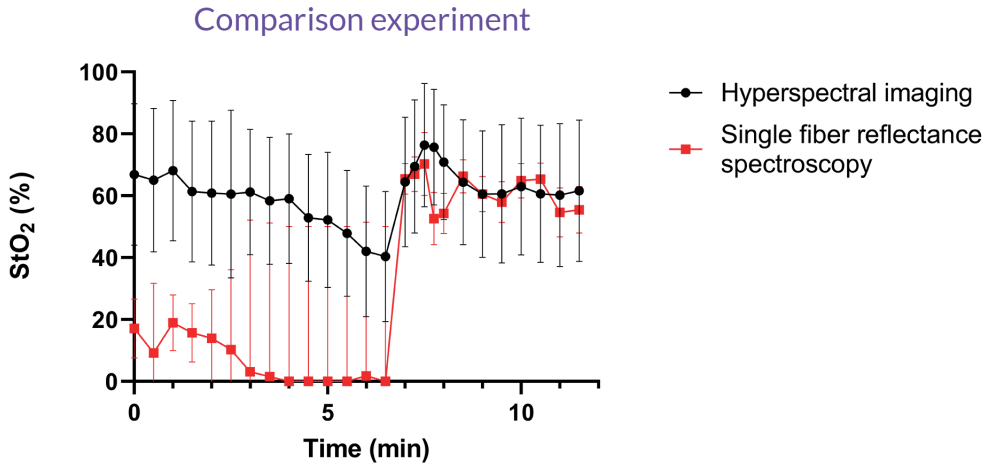

Figure 3. A typical example of the effect of vascular occlusion on superficial cutaneous oxygen saturation determined using hyperspectral imaging (color, saturation and saturation overlay maps) and perfusion determined by Laser Speckle Contrast Imaging (LSCI, perfusion maps).

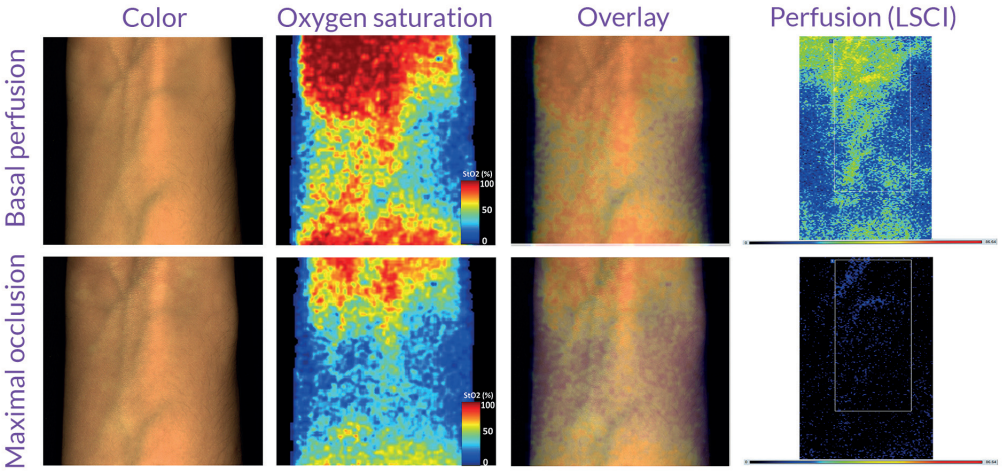

Figure 4. Correlation of cutaneous blood oxygen saturation with vascular perfusion during occlusion-reperfusion experiments in the LUMC cohort. Average of separate measurements of cutaneous blood oxygen saturation on measurement day 1 and 2 show a strong correlation with corresponding perfusion assessments by laser speckle imaging during occlusion-reperfusion experiments. Occlusion was performed after two minutes baseline measurements for a total of five minutes. Both oxygen saturation and blood flow levels returned to baseline after 12 minutes. *Abbreviations: AU: arbitrary units; StO_2: oxygen saturation.*

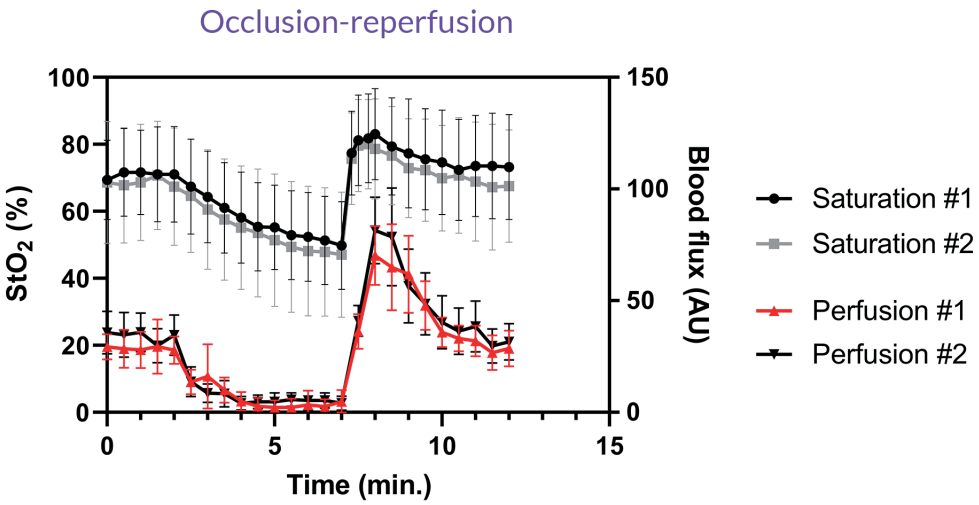

Figure 5. Tissue oxygen saturation levels after application of capsaicin cream, including subgroup analysis per cohort (LUMC *vs* MSKCC validation cohort). Cutaneous StO_2 levels did not change significantly after application of capsaicin in the most superficial layers. *Abbreviations: MSKCC: Memorial Sloan Kettering Cancer Center; LUMC: Leiden University Medical Center; StO_2: oxygen saturation.*

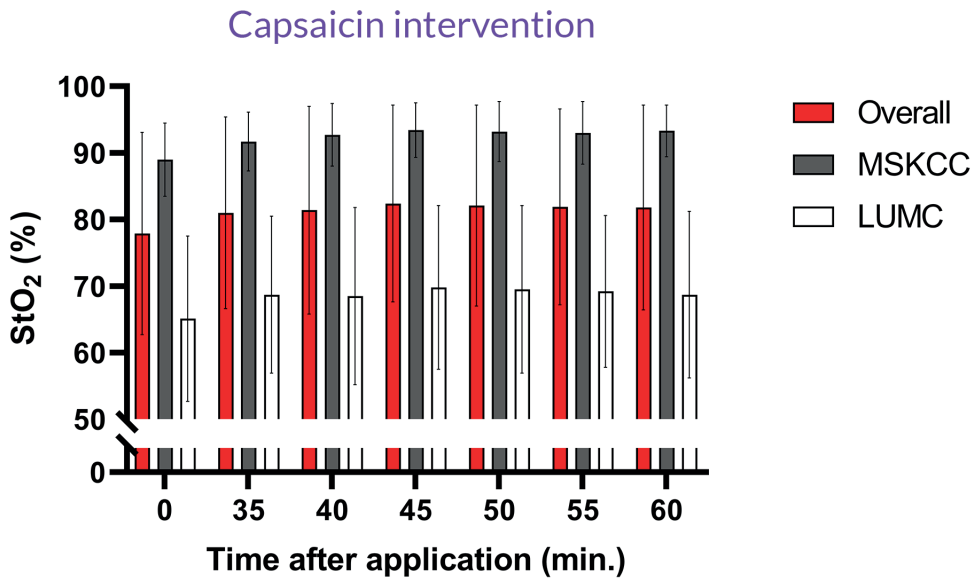

References

1. Arsenault KA, Al-Otaibi A, Devereaux PJ, Thorlund K, Tittley JG, Whitlock RP. The use of transcutaneous oximetry to predict healing complications of lower limb amputations: a systematic review and meta-analysis. *European journal of vascular and endovascular surgery : the official journal of the European Society for Vascular Surgery.* 2012;43(3):329-336.
2. Wilkins EG, Hamill JB, Kim HM, et al. Complications in Postmastectomy Breast Reconstruction: One-year Outcomes of the Mastectomy Reconstruction Outcomes Consortium (MROC) Study. *Annals of surgery.* 2018;267(1):164-170.
3. Yi J, Chen S, Backman V, Zhang HF. In vivo functional microangiography by visible-light optical coherence tomography. *Biomedical optics express.* 2014;5(10):3603-3612.
4. Lu G, Fei B. Medical hyperspectral imaging: a review. *Journal of biomedical optics.* 2014;19(1):10901.
5. Zherebtsov E, Dremin V, Popov A, et al. Hyperspectral imaging of human skin aided by artificial neural networks. *Biomedical optics express.* 2019;10(7):3545-3559.
6. Dremin V, Marcinkevics Z, Zherebtsov E, et al. Skin complications of diabetes mellitus revealed by polarized hyperspectral imaging and machine learning. *IEEE transactions on medical imaging.* 2021;Pp.
7. Kashani AH, Kirkman E, Martin G, Humayun MS. Hyperspectral computed tomographic imaging spectroscopy of vascular oxygen gradients in the rabbit retina in vivo. *PloS one.* 2011;6(9):e24482.
8. Gao L, Smith RT, Tkaczyk TS. Snapshot hyperspectral retinal camera with the Image Mapping Spectrometer (IMS). *Biomedical optics express.* 2012;3(1):48-54.
9. Amelink A, Robinson DJ, Sterenborg HJ. Confidence intervals on fit parameters derived from optical reflectance spectroscopy measurements. *Journal of biomedical optics.* 2008;13(5):054044.
10. Noguchi K, Matsuzaki T, Sakanashi M, et al. Effect of caffeine contained in a cup of coffee on microvascular function in healthy subjects. *Journal of pharmacological sciences.* 2015;127(2):217-222.
11. Gillespie JA. Vasodilator properties of alcohol. *British medical journal.* 1967;2(5547):274-277.
12. Manni F, van der Sommen F, Zinger S, et al. Hyperspectral Imaging for Skin Feature Detection: Advances in Markerless Tracking for Spine Surgery. *Applied Sciences.* 2020;10(12):4078.
13. Matheus ASM, da Matta MFB, Clemente ELS, Rodrigues MLG, Valenca DCT, Gomes MB. Sensibility and specificity of laser speckle contrast imaging according to Endo-PAT index in type 1 diabetes. *Microvascular research.* 2018;117:10-15.
14. Birkhoff WAJ, Heuberger J, Post TE, et al. Recombinant human erythropoietin does not affect several microvascular parameters in well-trained cyclists. *Physiological reports.* 2018;6(24):e13924.
15. Brooks S, Hoy CL, Amelink A, Robinson DJ, Nijsten TE. Sources of variability in the quantification of tissue optical properties by multidiameter single-fiber reflectance and fluorescence spectroscopy. *Journal of biomedical optics.* 2015;20(5):57002.
16. Hoy CL, Gamm UA, Sterenborg HJ, Robinson DJ, Amelink A. Method for rapid multidiameter single-fiber reflectance and fluorescence spectroscopy through a fiber bundle. *Journal of biomedical optics.* 2013;18(10):107005.
17. Stegehuis PL, Boogerd LS, Inderson A, et al. Toward optical guidance during endoscopic ultrasound-guided fine needle aspirations of pancreatic masses using single fiber reflectance spectroscopy: a feasibility study. *Journal of biomedical optics.* 2017;22(2):24001.
18. Buntinx L, Vermeersch S, de Hoon J. Development of anti-migraine therapeutics using the capsaicin-induced dermal blood flow model. *British journal of clinical pharmacology.* 2015;80(5):992-1000.
19. Toivonen ME, Rajani C, Klami A. Snapshot hyperspectral imaging using wide dilation networks. *Machine Vision and Applications.* 2020;32(1):9.
20. Amelink A, Bard MP, Burgers SA, Sterenborg HJ. Single-scattering spectroscopy for the endoscopic analysis of particle size in superficial layers of turbid media. *Applied optics.* 2003;42(19):4095-4101.
21. Middelburg TA, Kanick SC, de Haas ER, et al. Monitoring blood volume and saturation using superficial fibre optic reflectance spectroscopy during PDT of actinic keratosis. *Journal of biophotonics.* 2011;4(10):721-730.
22. Schober P, Boer C, Schwarte LA. Correlation Coefficients: Appropriate Use and Interpretation. *Anesthesia and analgesia.* 2018;126(5):1763-1768.
23. Barberio M, Longo F, Fiorillo C, et al. HYPerspectral Enhanced Reality (HYPER): a physiology-based surgical guidance tool. *Surgical endoscopy.* 2020;34(4):1736-1744.
24. Giannoni L, Lange F, Davies AL, et al. Hyperspectral Imaging of the Hemodynamic and Metabolic States of the Exposed Cortex: Investigating a Commercial Snapshot Solution. *Advances in experimental medicine and biology.* 2018;1072:13-20.
25. He Q, Liu T, Wang RK. Enhanced spatial resolution for snapshot hyperspectral imaging of blood perfusion and melanin information within human tissue. *Journal of biophotonics.* 2020;13(5):e202000019.
26. Rubins U, Marcinkevics Z, Cimurs J, Saknite I, Kviesis-Kipge E, Grabovskis A. Multimodal Device for Real-Time Monitoring of Skin Oxygen Saturation and Microcirculation Function. *Biosensors.* 2019;9(3).
27. Nkengne A, Robic J, Seroul P, Gueheunneux S, Jomier M, Vie K. SpectraCam(®) : A new polarized hyperspectral imaging system for repeatable and reproducible in vivo skin quantification of melanin, total hemoglobin, and oxygen saturation. *Skin research and technology : official journal of International Society for Bioengineering and the Skin (ISBS) [and] International Society for Digital Imaging of Skin (ISDIS) [and] International Society for Skin Imaging (ISSI).* 2018;24(1):99-107.
28. Zhang R, Verkruysse W, Choi B, et al. Determination of human skin optical properties from spectrophotometric measurements based on optimization by genetic algorithms. *Journal of biomedical optics.* 2005;10(2):024030.
29. Yudovsky D, Pilon L. Retrieving skin properties from in vivo spectral reflectance measurements. *Journal of biophotonics.* 2011;4(5):305-314.
30. Vyas S, Banerjee A, Burlina P. Estimating physiological skin parameters from hyperspectral signatures. *Journal of biomedical optics.* 2013;18(5):57008.
31. Jafari-Saraf L, Wilson SE, Gordon IL. Hyperspectral image measurements of skin hemoglobin compared with transcutaneous PO2 measurements. *Annals of vascular surgery.* 2012;26(4):537-548.
32. Chin MS, Freniere BB, Lo YC, et al. Hyperspectral imaging for early detection of oxygenation and perfusion changes in

irradiated skin. *Journal of biomedical optics.* 2012;17(2):026010.
33. Kabon B, Nagele A, Reddy D, et al. Obesity decreases perioperative tissue oxygenation. *Anesthesiology.* 2004;100(2):274-280.
34. Li M, Tang Y, Yao J. Photoacoustic tomography of blood oxygenation: A mini review. *Photoacoustics.* 2018;10:65-73.
35. Ghijsen M, Lentsch GR, Gioux S, et al. Quantitative real-time optical imaging of the tissue metabolic rate of oxygen consumption. *Journal of biomedical optics.* 2018;23(3):1-12.
36. Ghijsen M, Choi B, Durkin AJ, Gioux S, Tromberg BJ. Real-time simultaneous single snapshot of optical properties and blood flow using coherent spatial frequency domain imaging (cSFDI). *Biomedical optics express.* 2016;7(3):870-882.
37. IMEC (2021, April 2) https://www.imec-int.com/en/hyperspectral-imaging.
38. Geelen B, Tack N, Lambrechts A. *A compact snapshot multispectral imager with a monolithically integrated per-pixel filter mosaic.* Vol 8974: SPIE; 2014.